Research Article | Vol. 25, No. 3 | 6 Feb 2017 | OPTICS EXPRESS 2818

Optics EXPRESS

Proton radiation effect on InAs avalanche photodiodes

XINXIN ZHOU,[1] BENJAMIN WHITE,[1] XIAO MENG,[1,5] SHIYONG ZHANG,[1] MARINA GUTIERREZ,[2] MARK ROBBINS,[3,6] LUIS GOMEZ ROJAS,[3] NICK NELMS,[4] CHEE HING TAN,[1] AND JO SHIEN NG[1,*]

[1]*Department of Electronic and Electrical Engineering, University of Sheffield, Sheffield S3 7HQ, UK*
[2]*Departamento de Ciencia de los Materiales, Universidad de Ca´diz, 11510 Puerto Real, Spain*
[3]*Surrey Satellite Technology Ltd, Tycho House, Surrey Research Park, Guidlford GU2 7YE, UK*
[4]*Mechatronics and Optics Division, European Space Agency, ESTEC, P. O. Box 299, Netherlands*
[5]*Present address: School of Physics and Astronomy, Cardiff University, Cardiff CF24 3AA, UK*
[6]*Present address: e2v, 106, Waterhouse Lane, Chelmsford, Essex CM1 2QU, UK*
**j.s.ng@sheffield.ac.uk*

Abstract: With increasing interest over the past decade in space-related remote sensing and communications using near-infrared (NIR) wavelengths, there is a need for radiation studies on NIR avalanche photodiodes (APDs), due to the high radiation environment in space. In this work, we present an experimental study of proton radiation effects on performance parameters of InAs APDs, whose sensitivity extends from visible light to ~3.5 μm. Three irradiation energies (10.0, 31.4, and 58.8 MeV) and four fluences (10^9 to 10^{11} p/cm^2) were used. At the harshest irradiation condition (10.0 MeV energy and 10^{11} p/cm^2 fluence) the APDs' avalanche gain and leakage current showed a measurable degradation. However, the responsivity of the APDs was unaffected under all conditions tested. The data reported in this article is available from the figshare digital repository (DOI: https://dx.doi.org/10.15131/shef.data.4560562).

OCIS codes: (040.1345) Avalanche photodiodes (APDs); (120.6085) Space instrumentation.

References and links

1. A. Chédin, "The feasibility of monitoring CO_2 from high-resolution infrared sounders," J. Geophys. Res. **108**(D2), 4064 (2003).
2. R. T. Menzies and D. M. Tratt, "Differential laser absorption spectrometry for global profiling of tropospheric carbon dioxide: selection of optimum sounding frequencies for high-precision measurements," Appl. Opt. **42**(33), 6569–6577 (2003).
3. G. Ehret, C. Kiemle, M. Wirth, A. Amediek, A. Fix, and S. Houweling, "Space-borne remote sensing of CO_2, CH_4, and N_2O by integrated path differential absorption lidar: a sensitivity analysis," Appl. Phys. B **90**(3-4), 593–608 (2008).
4. D. S. G. Ong, J. S. Ng, Y. L. Goh, C. H. Tan, S. Zhang, and J. P. R. David, "InAlAs Avalanche Photodiode With Type-II Superlattice Absorber for Detection Beyond 2 μm," IEEE Trans. Electron Dev. **58**(2), 486–489 (2011).
5. J. Beck, T. Welch, P. Mitra, K. Reiff, X. Sun, and J. Abshire, "A highly sensitive multi-element HgCdTe e-APD detector for IPDA Lidar applications," J. Electron. Mater. **43**(8), 2970–2977 (2014).
6. A. R. J. Marshall, C. H. Tan, M. J. Steer, and J. P. R. David, "Electron dominated impact ionization and avalanche gain characteristics in InAs photodiodes," Appl. Phys. Lett. **93**(11), 111107 (2008).
7. P. J. Ker, A. R. J. Marshall, A. B. Krysa, J. P. R. David, and C. H. Tan, "Low noise high responsivity InAs avalanche photodiodes for infrared sensing," Phys. Status Solidi **9**(c), 310–313 (2011).
8. H. N. Becker, T. F. Miyahira, and A. H. Johnston, "The influence of structural characteristics on the response of silicon avalanche photodiodes to proton irradiation," IEEE Trans. Nucl. Sci. **50**(6), 1974–1981 (2003).
9. J. S. Laird, S. Onoda, T. Hirao, H. Becker, A. Johnston, and H. Itoh, "Effects of gamma and heavy ion damage on the impulse response and pulsed gain of a low breakdown voltage Si avalanche photodiode," IEEE Trans. Nucl. Sci. **53**(6), 3786–3793 (2006).
10. Y. C. Tan, R. Chandrasekara, C. Cheng, and A. Ling, "Silicon avalanche photodiode operation and lifetime analysis for small satellites," Opt. Express **21**(14), 16946–16954 (2013).

#281956 https://doi.org/10.1364/OE.25.002818
Journal © 2017 Received 1 Dec 2016; accepted 15 Jan 2017; published 2 Feb 2017

Optics EXPRESS

11. H. N. Becker and A. H. Johnston, "Dark current degradation of near infrared avalanche photodiodes from proton irradiation," IEEE Trans. Nucl. Sci. **51**(6), 3572–3578 (2004).
12. M. L. Dorn, J. L. Pipher, C. McMurtry, S. Hartman, A. Mainzer, M. McKelvey, R. McMurray, D. Chevara, and J. Rosser, "Proton irradiation results for long-wave HgCdTe infrared detector arrays for Near-Earth Object Camera," J. Astron. Telesc. Instrum. Syst. **2**(3), 036002 (2016).
13. G. P. Summers, E. A. Burke, P. Shapiro, S. R. Messenger, and R. J. Walters, "Damage correlations in semiconductors exposed to gamma, electron and proton radiations," IEEE Trans. Nucl. Sci. **40**(6), 1372–1379 (1993).
14. C. Inguimbert and R. Gigante, "NEMO: A code to compute NIEL of protons, neutrons, electrons, and heavy ions," IEEE Trans. Nucl. Sci. **53**(4), 1967–1972 (2006).
15. I. C. Sandall, J. S. Ng, S. Xie, P. J. Ker, and C. H. Tan, "Temperature dependence of impact ionization in InAs," Opt. Express **21**(7), 8630–8637 (2013).
16. V. V. Chaldyshev, A. L. Kolesnikova, N. A. Bert, and A. E. Romanov, "Investigation of dislocation loops associated with As-Sb nanoclusters in GaAs," J. Appl. Phys. **97**(2), 024309 (2005).

1. Introduction

Remote monitoring of greenhouse gases such as CO_2, CH_4 and NO_2 with global coverage and high spatial resolution constitutes a major part of studying the Earth's climate and its relationship with the changes introduced by human activities. Satellite-based atmospheric passive sounders using the infrared wavelengths provide gas concentration information mainly from the middle and upper troposphere due to their atmospheric weighting functions [1]. Using space-borne differential light detection and ranging (LIDAR) techniques, very accurate measurement of greenhouse gases within the lower troposphere, where the sinks and sources interact with the atmosphere, can be achieved [2, 3]. Hence differential LIDAR systems offer highly valuable information for the wider remote monitoring systems for greenhouse gases.

Performance of a differential LIDAR system for greenhouse gases depends on the performance of the laser and the optical detector used in the system as well as the operating wavelength. Considerations of atmospheric weighting functions that favor the lower troposphere, strong absorption peaks, optical depths and influence of temperature profile uncertainty on the deduced gas concentration led to several optimum wavelengths [2, 3]. These are ~1.6 μm (CO_2 and CH_4), ~2 μm (CO_2 and CH_4), and 3.9 μm (NO_2).

For operating wavelengths up to 1.6 μm, commercial detectors fabricated with $In_{0.53}Ga_{0.47}As$ photon absorption layers have suitable performance characteristics and so can be utilized. Furthermore, since the differential LIDAR systems are required to detect very weak optical signals with fast sample speeds, use of $In_{0.53}Ga_{0.47}As$ based APDs with acceptably low leakage currents can provide a marked improvement to the system's overall signal-to-noise ratio compared to a system employing a unity gain detector. For detection up to ~2 μm, an APD with an $In_{0.53}Ga_{0.47}As$/ $GaAs_{0.51}Sb_{0.49}$ type-II superlattice absorber and an $In_{0.52}Al_{0.48}As$ avalanche region was developed [4]. However photon absorption in type-II superlattice is an inherently inefficient process compared to direct bandgap materials. Hence APD technology based on type-II superlattice technologies is unlikely to yield quantum efficiency that is competitive with direct bandgap materials. Currently, the most promising APD technologies for ~2 μm wavelength detection are electron-APDs (e-APDs) made from either HgCdTe [5] or InAs [6, 7], both direct bandgap materials. These e-APDs provide avalanche gain without the usual penalty of avalanche noise, and their detection wavelengths extend up to 3.5 μm (InAs) or longer (depending on alloy composition of HgCdTe).

In addition to the usual APD performance parameters, when choosing APDs and designing radiation shields for space borne applications, considerations must be given to degradation of the APD performance brought on by exposure to radiation. Thus performance degradation of Si photodiodes and Si APDs due to radiation is well studied [8–10]. For infrared APDs, the only radiation damage study reported was on InGaAs/InP APDs and Ge APDs [11], even though there is a recent study on HgCdTe photodiodes (not e-APDs) [12]. For InAs, there has been no radiation report on either photodiodes or e-APDs.

Optics EXPRESS

Radiation damage studies carried out on Si, Ge and InGaAs/InP APDs concluded that the bulk of the noticeable radiation damage resulted from displacement damage [8–11]. Proton irradiation, which introduces ionization damage and displacement damage, is thus an appropriate choice of particles for such studies.

In this work, we investigate displacement damage effects on InAs APDs, by measuring changes in leakage current, responsivity and avalanche gain of the APDs subject to proton irradiation under three energies with four fluences.

2. Device fabrication and experimental detail

The InAs APDs used were grown by molecular beam epitaxy on a 2-inch n-type InAs substrate, with Be and Si as the p- and n- type dopant atoms. The expitaxial layers consist of a 300 nm p^+-layer (InAs and AlAsSb), a 3.5 μm InAs layer with graded p-doping, a 6.0 μm InAs i-layer and a 1.0 μm InAs n-layer, as shown schematically in Fig. 1(a). Circular mesa APDs with diameters of 400, 200, 100 and 50 μm, shown in Fig. 1(b), were fabricated on a sample piece cleaved from the wafer. Device fabrication used standard photolithography, Ti/Au (20/200 nm thick) ohmic contacts, and wet chemical etching solutions [6]. Finally mesa sidewalls were passivated using negative photoresist SU 8, minimizing surface leakage current.

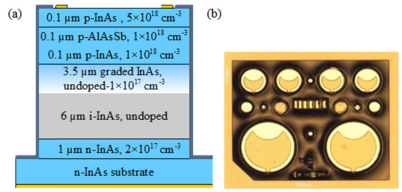

Fig. 1. (a) Structure of the InAs APD wafer and (b) top view of mesa InAs APDs.

Pre-irradiation APD characterization, carried out at 300 and 200 K (the intended operating temperature), included dark current versus reverse bias (I_d-V) characteristics in the dark, avalanche gain versus reverse bias ($M(V)$) characteristics, and responsivity at –0.2 V. The measurements of $M(V)$ and responsivity used modulated laser light at 1550 nm wavelength and phase-sensitive detection technique, to minimize influence of leakage currents. All measurements were carried out using probe stations so that no device packaging was needed for testing. When the pre-irradiation characterization was completed, the sample piece was cleaved into thirteen dies, labeled as Die #1 to Die #12, plus a reference die.

To investigate displacement damage, Dies 1 to 12 were irradiated by protons at the Proton Irradiation Facility at the Paul Scherrer Institute, whose staff performed the beam calibration and dosimetry. Three proton energies, 10.0, 31.4, and 58.8 MeV, and four fluences, Φ, 10^9 to 10^{11} p/cm^2, were used, as summarized in Table 1. In semiconductor devices, the extent of displacement damage-related performance degradation often appears to correspond to non-ionizing energy loss (NIEL), the equivalent average energy loss per unit path length caused by non-ionizing events (e.g. displacements of atoms) [13]. Hence NIEL values calculated using software from [14] are included in Table 1 for reference.

Table 1. Proton irradiation conditions, NIEL values and irradiated die numbers. Deduced damage factors for 200 K leakage currents of 200 μm diameter APDs are also listed.

Proton Energy (MeV)	Proton NIEL (keV/(g/cm^2))	Proton Fluence, Φ (proton/cm^2)				Damage factor, $\Delta I_d/\Phi$ (nA cm^2 /proton)	
		10^9	5×10^9	10^{10}	10^{11}	at –0.2 V (M = 1)	at –10 V (M = 22.8)
10.0	6.04	#1	#2	#3	#4	3.0×10^{-9}	1.5×10^{-7}
31.4	3.66	#5	#6	#7	#8	–	5.3×10^{-8}
58.8	3.85	#9	#10	#11	#12	–	1.2×10^{-7}

Optics EXPRESS

The irradiations were undertaken at room temperature without biasing the APDs on the dies. After the irradiation, characterization was repeated on all irradiated APD dies and the reference die, using identical conditions and setups as for pre-radiation tests. The measurements were completed within two weeks of the irradiations.

A large number of APDs were measured prior to and after the irradiation, as summarized in Table 2. The I_d-V characteristics covered the 400, 200 and 100 μm diameter APDs. The uniform dark current characteristics provide evidence of uniformity of APDs fabricated. Hence the $M(V)$ and responsivity measurements focused only on the 200 μm diameter APDs to ensure pure electron injection profiles are maintained in all measurements involving laser light, whilst dark currents remain sufficiently low. For each die, a minimum of 2 APDs were measured to obtain the mean $M(V)$ and responsivity. Hence all data shown are from the 200 μm diameter APDs. Sets of data obtained from the reference die prior to and after the proton irradiation were indistinguishable (within one standard deviation), confirming that the InAs APDs preserve their characteristics over the period so are sufficiently robust for proton irradiation effect(s) study.

Table 2. Number of APDs tested for each die prior to and after proton irradiation.

Measurements	Before irradiation		After irradiation	
	300 K	200 K	300 K	200 K
I_d-V	12	4 - 8	8-14	8-10
$M(V)$	≥ 2	≥ 2	≥ 2	≥ 2
Responsivity	≥ 2	≥ 2	≥ 2	≥ 2

3. APD performance prior to proton irradiation

Figure 2(a) and (b) plots the mean I_d-V and the mean $M(V)$ characteristics, respectively, with standard deviations from pre-radiation measurements at 300 and 200 K for APDs with diameters of 200 μm. For these APDs at 200 K, the mean I_d values were 150 nA at −0.2 V and 2.6 μA at −10 V. Dark currents at both temperatures were found to be dominated by diffusion currents, indicated by an activation energy, close to the bandgap, of 0.34 eV from temperature dependence analyses (temperature data points of 300, 250, 200 and 175 K).

The mean $M(V)$ characteristics with standard deviations at 300 and 200 K are compared in Fig. 2(b). The avalanche gain shows a positive temperature dependence, consistent with ref [15]. At 200 K, the avalanche gain at −10.0 V is 22.8 ± 0.3. Responsivity values, measured at −0.2 V, at 300 and 200 K are 0.62 ± 0.01 and 0.66 ± 0.01 A/W, respectively. As temperature decreases, the responsivity increases slightly, because of increased collection efficiency of photo-generated electrons (attributed to increased minority electron diffusion length in the top p-InAs layer).

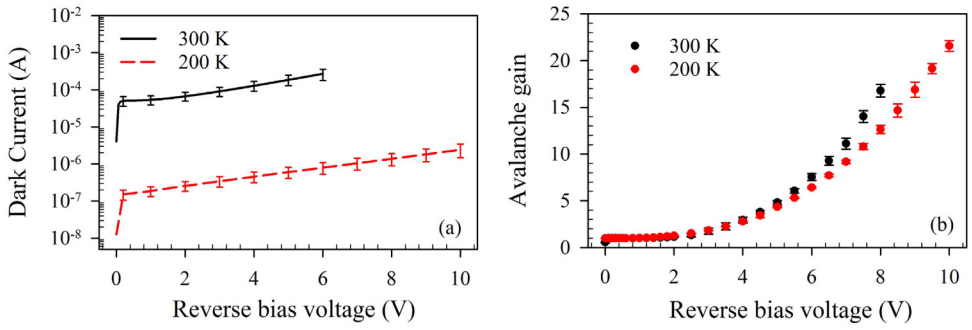

Fig. 2. (a) Mean I-V with standard deviations, and (b) mean $M(V)$ with standard deviations at 300 and 200 K of 200 μm diameter InAs APDs, prior to proton irradiation.

Optics EXPRESS

4. Dark currents after proton irradiation

In Fig. 3, mean I_d-V characteristics at 300 and 200 K from 200 μm diameter APDs from all irradiated dies are compared to the reference data presented in Fig. 2(a). At 300 K, out of the 12 irradiated dies, only APDs from Die #4 (10^{11} p/cm^2 at 10.0 MeV) showed a significant increase in dark current, at approximately 3 times larger compared to the reference APDs, at any given voltage. Observing Fig. 3(bottom row), the 200 K I_d-V characteristics comparisons reveal more significant degradation. Taking into account the error bars of the reference data, the 10.0 MeV proton irradiations cause degradation at any given voltage for the two largest Φ tested. For other proton energies, the I_d-V characteristic degrades only when the highest Φ was used, with the increase in I_d being voltage dependent.

Plotting the 200 K I_d values at −0.2 V and −10 V against Φ in Fig. 4(a) confirms that the 10.0 MeV protons caused the most significant degradation of I_d, followed by the 58.8 MeV protons and finally the 31.4 MeV protons.

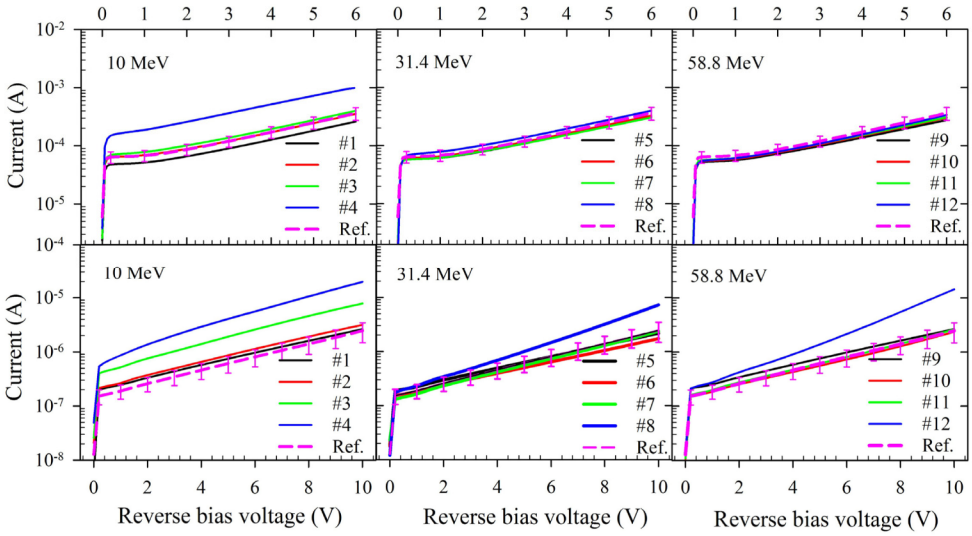

Fig. 3. Mean I-V characteristics at 300 (top row) and 200 K (bottom row) of the 200 μm diameter APDs from the proton-irradiated dies, along with the corresponding reference data (with standard deviations). Proton energies were 10.0 (left), 31.4 (middle), and 58.8 (right) MeV.

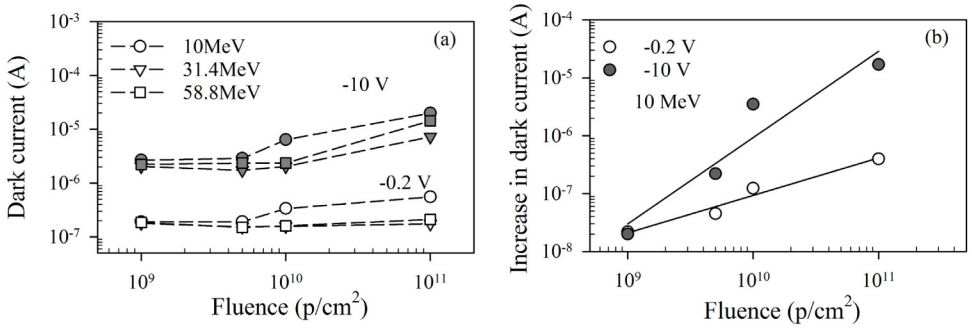

Fig. 4. (a) I_d at −0.2 and −10 V versus fluence for all irradiated dies, and (b) ΔI_d at −0.2 and −10 V versus fluence for dies irradiated with 10.0 MeV protons. All data are for 200 μm diameter APDs at 200 K.

Optics EXPRESS

Next we analyze the increase in 200 K dark currents (with respect to the reference APDs), ΔI_d, versus Φ. For Dies #1, #2, #3, and #4 (10.0 MeV), ΔI_d are shown in Fig. 4(b), for reverse bias of −0.2 and −10 V. For a given reverse bias, the data can be fitted with a linear equation with $\Delta I_d/\Phi$ as the gradients. Values of $\Delta I_d/\Phi$ for the 200 μm diameter APDs cooled to 200 K at −0.2 and −10 V are given in Table 1. A larger reverse bias produced a larger $\Delta I_d/\Phi$, which is at least partially caused by a higher M amplifying ΔI_d, and a wider depletion region (from 1.9 to 7.6 μm) that increases the number of damage-related defects [8].

When higher proton energy was used, the dark current increases beyond the error bars of the reference data only when fluence of 10^{11} p/cm^2 was used (Dies #8 and #12). Thus the damage threshold fluence for dark current at 31.8 and 58.8 MeV proton energy is noticeable higher than that at 10.0 MeV.

To assess possible unbiased room temperature annealing, a further round of post irradiation 200 K dark current measurements on the reference die, Die #3, and Die #4 was carried out 4 months after the irradiations (results not shown here). The dies were kept at room temperature in between both sets of tests. At −0.2 V, the dark currents of all APDs were found to be indistinguishable from the measurements carried out within the first 2 weeks of proton irradiation. At −10.0 V, the reference die had a mean dark current of ~2.6 μA (200 μm diameter APD), which is consistent with Fig. 3 showed negligible change. At the same reverse bias voltage, the dark currents of APDs from Die #3 and Die #4 were found to decrease from 7.8 to 4.2 μA and 21 to 13 μA, respectively. The extent of the recovery is significant, however, APDs from both dies still had higher dark currents than the reference APDs by a factor of ~1.6 and 5.2, respectively.

5. Responsivity and $M(V)$ after proton irradiation

Despite the radiation-induced bulk damage causing an increase in dark current for some of the dies, the intrinsic photon absorption and photo-generated current collection efficiency in the InAs APDs appears to be unaffected. This is evidenced by the negligible difference in responsivity values (taken at −0.2 V) before and after the proton irradiation, as compared in Figs. 5(a) and 5(b), for 300 and 200 K, respectively.

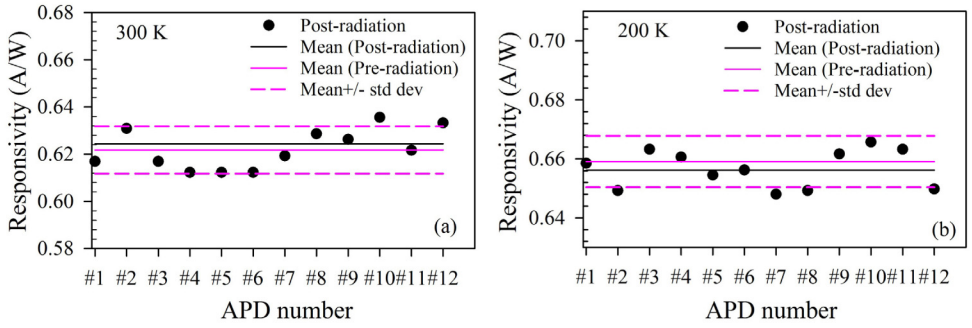

Fig. 5. Responsivity at −0.2 V of the dies at (a) 300 and (b) 200 K, compared to the reference values (with standard deviations).

Optics EXPRESS

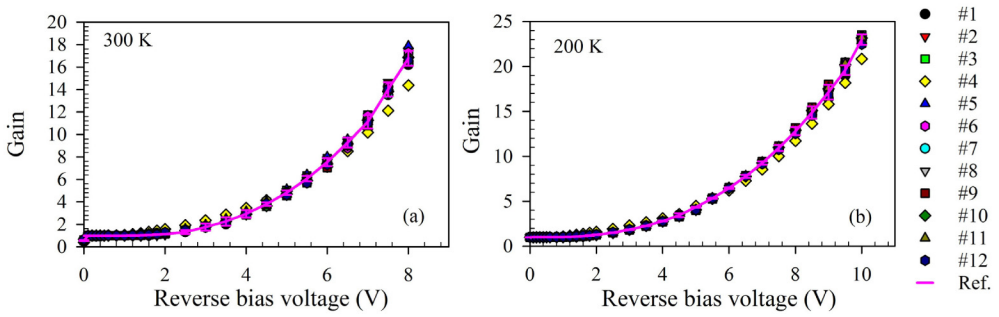

Fig. 6. Avalanche gain versus reverse bias of all dies at (a) 300 and (b) 200 K, compared to the reference values (with standard deviations).

For $M(V)$ data, pre- and post-irradiation data compared in Figs. 6(a) and 6(b), for 300 and 200 K, respectively, shows that all irradiated dies exhibit $M(V)$ highly similar to the reference data from pre-radiation measurements, except for Die #4, which exhibits the highest ΔI_d. It is possible that the level of displacement damage in Die #4 has led to an altered doping profile and hence electric field profile in the devices, giving rise to a slightly different $M(V)$ characteristics.

6. Damage analysis

Using a different pair of InAs APD samples with Be-doped p-layer and thick i-layers, Transmission Electron Microscopy (TEM) studies were carried out as part of this work. One of the samples was irradiated at the same time as Die #4, which has shown the worst degradation in device performance, and the other was not irradiated so serves as a reference sample.

To observe the presence of radiation-induced defects in the samples, 220 bright field TEM images were taken from both samples. The reference sample was found to be free of extended defects. However, the TEM image of the irradiated sample revealed dislocation loops in the p-doped InAs layer (within 750 nm from the top of the sample), as shown in Fig. 7(a). These loops were further studied using high-resolution TEM (HREM). In all of them, a Moiré fringe area was identified as a precipitate that gives rise to the dislocation loop [16]. A typical HREM image of a dislocation loop in Fig. 7(a) is shown in Fig. 7(b), where a rectangle and a dotted ellipse indicate the Moiré fringe area and the dislocation loop, respectively. These defects are likely to be present in Die #4 too, so may have contributed to the increased dark currents and altered $M(V)$ characteristics (Sections 5 and 6).

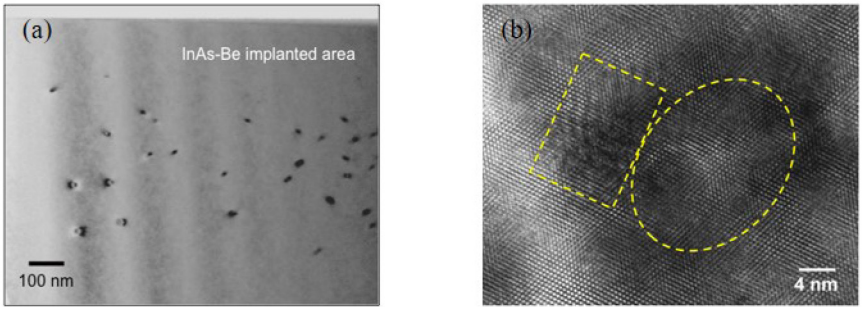

Fig. 7. An InAs sample irradiated with the same condition as Die #4, showing (a) dislocation loops within the p-doped layer in a bright field TEM image, and (b) a Moiré fringe area (rectangle) and a dislocation loop (ellipse) in a HREM image.

Optics EXPRESS

7. Conclusions

An experimental study of effects of proton irradiation on InAs APDs developed for detecting 2 to 3 μm wavelength light was conducted. The study used InAs APDs with a mesa topology and assessed dark current, avalanche gain and responsivity, measured at 300 and 200 K. Of the three parameters, the dark currents showed the most significant degradation. At 300 K, only the harshest irradiation condition (10.0 MeV energy and 10^{11} p/cm^{2}fluence) caused an increase in dark currents. At 200K, however, dark currents increased when proton energy was 10.0 MeV and fluence reached 10^{10} p/cm^2. With proton energies of 31.8 and 58.8 MeV, the damage threshold for dark current was higher (fluence ≥ 10^{11} p/cm^2).

No noticeable change was found for responsivity, despite presence of dislocation loops within the p-InAs layer of the sample irradiated with the harshest condition. For avalanche gain, none of the irradiation conditions resulted in degradation, except for a slight change for the harshest condition. At 10.0 MeV and fluence of 10^{11} p/cm^2, the avalanche gain at −10.0 V and 200 K reduced from 22.8 to 20.8.

Funding

UK Engineering and Physical Sciences Research Council (EPSRC) (EP/H031464/1); European Space Agency (ESA) (4000107110/12/NL/CBi); Royal Society (University Research Fellowship for J. S. Ng).